

Dynamics of random replicators with Hebbian interactions

Tobias Galla^{†‡}

[†] The Abdus Salam International Centre for Theoretical Physics, Strada Costiera 11, 34014 Trieste, Italy

[‡] INFN/CNR, Trieste-SISSA Unit, V. Beirut 2-4, 34014 Trieste, Italy

Abstract. A system of replicators with Hebbian random couplings is studied using dynamical methods. The self-reproducing species are here characterized by a set of binary traits and interact based on complementarity. In the case of an extensive number of traits we use path-integral techniques to demonstrate how the coupled dynamics of the system can be formulated in terms of an effective single-species process in the thermodynamic limit, and how persistent order parameters characterizing the stationary states may be computed from this process in agreement with existing replica studies of the statics. Numerical simulations confirm these results. The analysis of the dynamics allows an interpretation of two different types of phase transitions of the model in terms of memory onset at finite and diverging integrated response, respectively. We extend the analysis to the case of diluted couplings of an arbitrary symmetry, where replica theory is not applicable. Finally the dynamics and in particular the approach to the stationary state of the model with a finite number of traits is addressed.

PACS numbers: 87.23-n, 87.10+e, 75.10.Nr, 64.60.Ht

E-mail: galla@ictp.trieste.it

1. Introduction

The dynamics and collective phenomena of interacting agents in models of game theory, economy and biology are currently studied intensively in the physics community for example in the context of the so-called Minority Game [1, 2, 3]. In particular the tools of equilibrium and non-equilibrium statistical mechanics have proved to be extremely powerful for the analysis of such complex systems with many degrees of freedom. Another prominent example of such systems consists in so-called replicator models (RM) which are commonly used to describe the evolution of self-reproducing interacting species competing within a given framework of limited resources. RM have found wide applications in a variety of fields including game theory, socio-biology, pre-biotic evolution and optimization theory [4, 5]. While earlier studies were mostly restricted to the deterministic case the first model with random interactions, the so-called random replicator model (RRM), was introduced by Diederich and Oppen in [6, 7]. The

randomness of the interspecies couplings here reflects an amount of uncertainty about the structure of interactions in real ecosystems. The initial RRM and various extensions have subsequently been studied in a series of papers [8, 9, 10, 11, 12, 13, 14, 15, 16, 17] and they have been found to exhibit intriguing features, both from the biological point of view as well as from the perspective of statistical mechanics. In particular it has been realised that the model exhibits phase behaviour with interesting ergodic and non-ergodic phases, different types of phase transitions as well as replica-symmetry breaking.

From the point of view of statistical mechanics, RRMs can be seen as disordered complex systems with quenched random couplings. The variations of RRMs mentioned above then differ in the details of the statistics from which the couplings are drawn. In the original model of Diederich and Oppen the interactions between the species were assumed to be pairwise and drawn from a Gaussian distribution, [9] discusses the case of higher-order Gaussian interactions and [11], [12] and [13] are concerned with models in which the couplings are of a separable Hebbian structure, reminiscent of those used extensively in the context of neural networks [18, 19].

Most of this existing work on RRM in the physics literature seems to focus on either numerical simulations and/or on the application of static methods borrowed from statistical mechanics, most notably replica techniques. The only exception in which exact dynamical techniques are employed to deal with the disordered interactions of RRM appears to be the early paper [7] by Oppen and Diederich (and the follow-up [8]) and the work by Rieger [20], where RRM are addressed using dynamical generating functionals à la De Dominicis [21]. The use of replica methods to study the statics of such models relies on the existence of a global Lyapunov (or fitness) function, the stationary states of the replicator system are then identified as extrema of this random function. This, however, constitutes a severe constraint from the point of view of biology as it limits the accessible systems to those with symmetric couplings. Models with (even partial) asymmetry in the interactions do not allow one to formulate the dynamics in terms of a Lyapunov function so that replica techniques can not be applied in this case. Hence, under such circumstances a direct study of the dynamics of the systems is required.

In this paper we discuss a dynamical approach to a class of RRM with Hebbian interactions. In the fully connected case the inter-species interactions are purely symmetric so that we can compare the results we obtain from a generating functional approach to earlier analyses of the statics of the same model [12, 13]. In particular we show that both methods lead to the same equations for the observables describing the stationary states. The study of the dynamics however enables us to shed some additional light on the two different types of phase transitions previously observed in the statical analysis of the model, and allows for an interpretation of these transitions in terms of an instability of the fixed point reached, and equivalently in terms of ergodicity breaking, dependence on initial conditions and of memory onset. We then extend the analysis to cases of Hebbian couplings with dilution of an arbitrary symmetry, where replica theory is no longer applicable. Finally a discussion of the dynamics of the model

with a finite number of traits is presented. Here we can go beyond the computation of the statistics of fixed-point solutions and can make statements regarding the approach to the stationary state.

2. Model definitions

The basic ingredients of the model are as follows. We consider a population of N species, labelled by Roman indices $i = 1, \dots, N$, and with concentrations $x_i \in [0, \infty)$. The system evolves in time according to the following replicator equations

$$\frac{d}{dt}x_i(t) = -x_i(t) \left[\sum_{j=1}^N \frac{c_{ij}}{c} J_{ij} x_j(t) + \sigma \zeta_i(t) - \lambda(t) \right]. \quad (1)$$

Here J_{ij} denotes the coupling between species i and j , $J_{ij} < 0$ corresponds to a pair of co-operating species, whereas i and j are competing with each other, if $J_{ij} > 0$. The $c_{ij} \in \{0, 1\}$ specify the dilution of the interactions, they are drawn such that any given link c_{ij} is present with probability $c \in (0, 1]$, further details of their distribution will be given below. Following [12, 13] each species i is then assumed to carry P traits, ξ_i^μ , labelled by an index $\mu = 1, \dots, P$. In the first part of the paper we will take the number of traits to be proportional to the system size, i.e. $P = \alpha c N$, where $\alpha = \mathcal{O}(1)$ is an additional model parameter. The case $P = \mathcal{O}(1)$ is discussed in the final section before the conclusions. The traits $\{\xi_i^\mu\}$ take values $\{-1, 1\}$ with equal probability and are drawn independently before the dynamics is started and then remain fixed. The interaction between species is then given by the Hebb rule

$$J_{ij} = \frac{1}{N} \sum_{\mu=1}^{\alpha c N} \xi_i^\mu \xi_j^\mu, \quad i \neq j, \quad (2)$$

Two species i and j are the more co-operative, the more complementary traits μ with $\xi_i^\mu \xi_j^\mu = -1$ they have. If i and j carry a large number of identical traits, they will be competitors. The traits $\{\xi_i^\mu\}$ along with the dilution variables $\{c_{ij}\}$ represent the quenched disorder of the problem. The latter are drawn from a distribution with the following statistics ($i \neq j$):

$$c = \langle c_{ij} \rangle_c = \langle c_{ji} \rangle_c, \quad \langle c_{ij} c_{ji} \rangle_c - c^2 = \Gamma c(1 - c) \quad (3)$$

($\langle \dots \rangle_c$ stands for an average over the dilution variables). $c \in (0, 1]$ denotes the connectivity, we here focus on the case of extensively many connections per species ($cN \sim \mathcal{O}(N)$). The parameter Γ controls the symmetry of the dilution, for $\Gamma = 1$ one has $c_{ij} = c_{ji}$, whereas c_{ij} and c_{ji} are uncorrelated for $\Gamma = 0$. Choosing $0 \leq \Gamma \leq 1$ allows one to interpolate between these two cases. For $c = 1$ the parameter Γ becomes irrelevant and we recover the fully connected model studied by static means in [12, 13]. We set $c_{ii} = 1$ and the diagonal elements J_{ii} are fixed to

$$J_{ii} = 2u, \quad (4)$$

where $u \geq 0$ stands for the self-interaction, or so-called co-operation pressure [7, 4]. The scaling of the self-interaction with c is chosen similar to the choice of [13]‡ and accordingly we do not address the so-called ‘extremely dilute limit’ $\lim_{N \rightarrow \infty} c = 0$ while still $\lim_{N \rightarrow \infty} cN = \infty$ sometimes considered in the context of neural networks [18, 19]. u is an additional model parameter, large values of the self-interaction will favour states in which all species concentrations remain positive whereas for small u the disordered non-diagonal terms J_{ij} dominate the interactions and some fraction of the species may die out asymptotically. The $\{\zeta_i(t)\}$ in (1) represent Gaussian white noise of zero mean and unit variance, so that the concentration of each species is subject to random fluctuations of magnitude σ . We will mostly concentrate on the case $\sigma = 0$ but consider $\sigma > 0$ to study the stability of the solutions of the noiseless dynamics. Finally, the Lagrange parameter $\boldsymbol{\lambda} = \{\lambda(t)\}$ is chosen to ensure the normalization

$$\sum_{i=1}^N x_i(t) = N \quad (5)$$

at all times, so that the total concentration of species is kept constant as the eco-system evolves in time. We note that in absence of the noise $\zeta_i(t)$ Eq. (1) may be written as

$$\frac{d}{dt} x_i(t) = x_i(t) [f_i(t) + \lambda(t)], \quad (6)$$

where $f_i(t) = -\sum_j (c_{ij}/c) J_{ij} x_j(t)$ is the ‘fitness’ of species i at time t . The normalization constant $\lambda(t)$ is then related to the ‘mean fitness’ by

$$\lambda(t) = -\frac{1}{N} \sum_j x_j(t) f_j(t). \quad (7)$$

In terms of game theory the variables i can be understood to label different strategies and $x_i(t)$ as the fraction of individuals playing strategy i at time t in a given population of agents. A player playing strategy i in an ensemble characterized by the vector $\mathbf{x} = (x_1, \dots, x_N)$ then receives a payoff $f_i(\mathbf{x}(t))$. Any individual i is assumed to reproduce at a rate proportional to the difference between $f_i(t)$ and the mean fitness across the population at time t . All offsprings of individual i then inherit the strategy of i .

3. Generating functional analysis

3.1. Generating functional and single effective species process

In the thermodynamic limit the time-evolution of the N coupled replicator equations (1) is conveniently studied using generating functional techniques originally developed for disordered systems by De Dominicis [21]. These allow one to express dynamics in terms of macroscopic order parameters such as the correlation and response functions of the system and have proved to be extremely powerful not only for the analysis of

‡ The analysis can be adapted to the case $(c_{ii} J_{ii})/c = 2u = \mathcal{O}(c^0)$ upon replacing $u \rightarrow uc$ throughout the calculation.

spin-glasses and neural networks, but for example also in the context of the Minority Game and other agent-based models [2]; generating functionals have also been used to study simple cases of RRM in [7, 20]. In order to generate response functions we first add perturbation fields $\{h_i(t)\}$ to the replicator dynamics and start from

$$\frac{d}{dt}x_i(t) = -x_i(t) \left[\sum_{j=1}^N \frac{c_{ij}}{c} J_{ij} x_j(t) + \sigma \zeta_i(t) - \lambda(t) + h_i(t) \right]. \quad (8)$$

The generating functional is then defined as

$$\begin{aligned} Z[\boldsymbol{\psi}] &= \left\langle e^{i \sum_i \int dt x_i(t) \psi_i(t)} \right\rangle_{\text{paths}} \\ &\equiv \int D\mathbf{x} D\hat{\mathbf{x}} p(\mathbf{x}(0)) \exp \left[i \sum_i \int dt \hat{x}_i(t) \left(\sum_{j=1}^N \frac{c_{ij}}{c} J_{ij} x_j(t) \right) \right] \\ &\times \exp \left[i \sum_i \int dt \hat{x}_i(t) (\dot{y}_i(t) - \lambda(t) + \sigma \zeta_i(t) + h_i(t)) \right]. \end{aligned} \quad (9)$$

Following [7] we have here employed a transformation $y_i(t) = \log x_i(t)$ (for $x_i(t) > 0$) in order to bring the replicator equations into a suitable form. Note that any x_i which is initialized at $x_i(t=0) = 0$ will remain zero forever. The functional $Z[\boldsymbol{\psi}]$ (with $\boldsymbol{\psi} = \{\boldsymbol{\psi}(t)\}_{t \geq 0} = \{(\psi_1(t), \dots, \psi_N(t))\}_{t \geq 0}$) thus represents the Fourier transform of the measure describing the probability of a certain path $\{\mathbf{x}(t) = (x_1(t), \dots, x_N(t))\}_{t \geq 0}$ to occur. $p(\mathbf{x}(0))$ describes the distribution of initial conditions from which the dynamics is started at time $t = 0$. Once the disorder-averaged generating functional $\overline{Z[\boldsymbol{\psi}]}$ has been computed, correlation and response functions may be obtained by taking derivatives $\overline{Z[\boldsymbol{\psi}]}$ of with respect to the source and perturbation fields $\{\psi_i(t), h_i(t)\}$.

The procedure of performing the disorder-average in the thermodynamic limit $N \rightarrow \infty$ is standard [7, 19, 2] and results in a self-consistent closed system of equations for the dynamical order parameters of the problem. For the present system these order parameters are given by the Lagrange parameter $\boldsymbol{\lambda} = \{\overline{\langle \lambda(t) \rangle}\}$ and the correlation and response functions $\{\mathbf{C}, \mathbf{G}\}$:

$$C(t, t') = \lim_{N \rightarrow \infty} \frac{1}{N} \sum_{i=1}^N \overline{\langle x_i(t) x_i(t') \rangle}, \quad G(t, t') = \lim_{N \rightarrow \infty} \frac{1}{N} \sum_{i=1}^N \frac{\delta \overline{\langle x_i(t) \rangle}}{\delta h_i(t')}. \quad (10)$$

Here $\langle \dots \rangle$ denotes an average over the possibly random initial conditions and over realisations of the white noise variables $\{\zeta_i(t)\}$. Note that $G(t, t') = 0$ for $t \leq t'$ due to causality, and that in general we expect the $G(t, t')$ to take negative values, given the effective sign of the perturbation $h_i(t)$ in (8). Unlike in the case of spherical models of spin-glasses [22] no explicit closed differential equations for $\{\boldsymbol{\lambda}, \mathbf{C}, \mathbf{G}\}$ can be found in the present model. Instead the order parameters are to be computed self-consistently from a non-Markovian stochastic process for an effective single-species concentration $x(t)$. This process turns out to be given by

$$\frac{d}{dt}x(t) = -x(t) \left(\frac{2u}{c} x(t) + \alpha \int_0^t dt' [c\mathbf{G}(\mathbb{I} - \mathbf{G})^{-1} + \Gamma(1-c)\mathbf{G}](t, t') x(t') \right)$$

$$- \lambda(t) + h(t) + \sigma \zeta(t) + \eta(t) \Big). \quad (11)$$

Here we have assumed that the distribution of initial conditions $p(\mathbf{x}(0))$ factorizes over the individual species $\{i\}$ and that the perturbation fields $\{h_i(t)\}$ take the form $h_i(t) \equiv h(t)$ for all i . $\{\eta(t)\}$ is Gaussian coloured noise with temporal correlations

$$\alpha \Lambda(t, t') \equiv \langle \eta(t) \eta(t') \rangle = \alpha [c(\mathbb{I} - \mathbf{G})^{-1} \mathbf{C} (\mathbb{I} - \mathbf{G}^T)^{-1} + (1 - c) \mathbf{C}] (t, t'). \quad (12)$$

\mathbb{I} denotes the identity matrix, and $\{\zeta(t)\}$ is white noise of zero mean and unit variance and reflects the white noise present in the original multi-species problem. The above correlation and response functions \mathbf{C} and \mathbf{G} can in turn be shown to be given by

$$C(t, t') = \langle x(t) x(t') \rangle_\star, \quad G(t, t') = \frac{\delta}{\delta h(t')} \langle x(t) \rangle_\star, \quad (13)$$

and $\boldsymbol{\lambda} = \{\lambda(t)\}$ has to be chosen such that

$$\langle x(t) \rangle_\star = 1 \quad \forall t, \quad (14)$$

corresponding to the constraint (5) in the original dynamics §. Here $\langle \dots \rangle_\star$ denotes an average over realisations of the effective process (11), i.e. over realisations of the single-species coloured noise $\{\eta(t)\}$ and the white noise $\{\zeta(t)\}$. The perturbation field $h(t)$ served us only to generate response functions, and will be set to zero from now on. Note also that (up to a sign) $G(t, t')$ may equivalently be obtained by taking a derivative of $\langle x(t) \rangle_\star$ with respect to $\lambda(t)$.

Eqs. (11,12,13,14) thus form a closed set of equations from which $\{\boldsymbol{\lambda}, \mathbf{C}, \mathbf{G}\}$ are to be obtained. These equations are exact and fully equivalent to the original N -species problem Eq. (1) in the limit $N \rightarrow \infty$. The retarded self-interaction and the coloured noise are a direct consequence of the quenched disorder in the original problem and impede an explicit analytical solution of the self-consistent saddle-point equations for the full two-time objects \mathbf{C}, \mathbf{G} and the function $\boldsymbol{\lambda}$. In similar disordered systems (such as the Minority Game) one therefore has to resort to specific ansätze for the trajectories of the effective particles [2]. Alternatively, effective dynamical problems in discrete time may be addressed using a Monte-Carlo integration of the resulting non-Markovian single-particle processes [23]. While this method allows one to compute the dynamical order parameters numerically without finite-size effects the iteration quickly becomes costly in terms of computer time as the number of time-steps is increased. For similar disordered systems one is usually limited to $\mathcal{O}(100)$ iterations, the equilibration times for suitably discretised versions of the present system however turn out to be much larger.

§ Technically speaking we here only demand that the relation $\lim_{N \rightarrow \infty} N^{-1} \sum_i \overline{\langle x_i \rangle} = 1$ be satisfied. For $N \rightarrow \infty$ the differences between the condition (5) imposed on any sample of the original process and this softer constraint are expected to be irrelevant; see also [2] for a similar case in the context of spherical Minority Games.

3.2. Stationary state

In order to proceed we assume that a stationary time-translation invariant state is reached in the long-term limit, i.e. we will be looking for solutions of the following type

$$\lim_{t \rightarrow \infty} C(t + \tau, t) = C(\tau), \quad \lim_{t \rightarrow \infty} G(t + \tau, t) = G(\tau), \quad \lim_{t \rightarrow \infty} \lambda(t) = \lambda. \quad (15)$$

Furthermore we will only address ergodic stationary states, that is states in which perturbations have no long-term effects so that the integrated response function

$$\chi \equiv \int_0^\infty d\tau G(\tau) \quad (16)$$

remains finite, $|\chi| < \infty$, and so that no long-term memory is present, i.e. we will assume

$$\lim_{t \rightarrow \infty} G(t, t') = 0 \quad \forall t'. \quad (17)$$

Note again that with the present definitions we expect χ to be negative in general, as the perturbation $h_i(t)$ effectively acts with a negative sign on \dot{x}_i in Eq. (8). At this stage a specific ansatz needs to be made to address the stationary states reached by the effective process. We will henceforth restrict the analysis to the case $\sigma = 0$, in which the original problem (1) becomes fully deterministic once the disordered interactions and random initial conditions have been drawn. In this case it conveniently turns out in simulations that all trajectories $\{x_i(t)\}$ evolve into fixed points $x_i \equiv \lim_{t \rightarrow \infty} x_i(t)$ for all i for large enough values of u . This observation simplifies the analysis considerably, as we may now accordingly look for solutions $x(t) \rightarrow x$ of the effective process, resulting in a flat correlation function

$$q \equiv C(\tau) \quad \forall \tau \quad (18)$$

in the stationary state. $1/q$ here serves as a measure of the diversity of the system, large values of $1/q \approx 1$ indicate a large fraction of surviving species with roughly equal concentrations ($x_i \approx 1 \quad \forall i$), for small $1/q \ll 1$ only a small number of species survives asymptotically in the present model (in the present model the number of surviving species is extensive); see also [10] for further details of the interpretation of $1/q$. Within the fixed point ansatz we also assume that the single-species noise $\{\eta(t)\}$ approaches a time-independent value η , which in turn is a static Gaussian random variable of zero mean and variance (cf. Eq. 12))

$$\langle \eta^2 \rangle = \alpha \left(c \frac{q}{(1-\chi)^2} + (1-c)q \right). \quad (19)$$

We abbreviate $\Sigma^2 \equiv \alpha \left(c \frac{q}{(1-\chi)^2} + (1-c)q \right)$ from now on. Any particular realization of $\eta(t)$ in the effective process thus leads to a realization of the random variable η , which

|| In the case of symmetric couplings ($c = 1$ or $\Gamma = 1$) this statement holds for all u . This is due to the existence of a Lyapunov function governing the dynamics, and similar behaviour has been observed in RRM with Gaussian symmetric couplings [8]. In the case of asymmetric couplings fixed point solutions are generally only found in the regime of large self-interaction u , larger than a critical value u^* which depends on the details of the model [8].

in turn determines the value of the fixed point x reached by that particular trajectory of the effective process. In the following we write $\eta = \Sigma z$ with z a standard Gaussian variable. Note that for the moment we will only assume the existence of such fixed points, their local stability against perturbations will be discussed in detail below.

Inserting this ansatz into the effective process (11) one finds (for $h(t) = 0$)

$$x \left(\frac{2u}{c} x + \alpha \left(c \frac{\chi}{1-\chi} + \Gamma(1-c)\chi \right) x - \lambda + \Sigma z \right) = 0, \quad (20)$$

and we conclude that the random variable x can take values of either $x = 0$ or $x = \frac{\lambda - \Sigma z}{\frac{2u}{c} + \alpha \left(c \frac{\chi}{1-\chi} + \Gamma(1-c)\chi \right)}$, depending on z . Given that $x(t) \geq 0$ the latter solution can only be realised provided that $z < \Delta$, where $\Delta = \lambda/\Sigma$ (the denominator $\frac{2u}{c} + \alpha \left(c \frac{\chi}{1-\chi} + \Gamma(1-c)\chi \right)$ comes out positive), so that we write

$$x(z) = \frac{\lambda - \Sigma z}{\frac{2u}{c} + \alpha c \frac{\chi}{1-\chi} + \Gamma(1-c)\chi} \Theta[\lambda - \Sigma z], \quad (21)$$

following [7], with $\Theta(y)$ the step-function, i.e. $\Theta(y) = 1$ for $y > 0$ and $\Theta(y) = 0$ otherwise. We note here that $x(z) = 0$ is a solution of (20) for all values of z . As it will turn out later (see Eq. (31)) these zero fixed points are unstable against perturbations if $\lambda - \Sigma z > 0$, which justifies (21) *a posteriori*. Note also that we choose initial conditions such that $x_i(0) > 0$ with probability one for all i , as concentrations set to zero from the start remain zero throughout the dynamics.

Using (21) the self-consistency requirements (13) and (14) translate into the following relations:

$$q = \langle x^2 \rangle_{\star}, \quad \chi = - \left\langle \frac{\partial x}{\partial \lambda} \right\rangle_{\star}, \quad \langle x \rangle_{\star} = 1. \quad (22)$$

In explicit form these may be written as

$$\left[\alpha \left(\frac{cq}{(1-\chi)^2} + (1-c)q \right) \right]^{-1/2} \left[\frac{2u}{c} + \alpha \left(c \frac{\chi}{1-\chi} + \Gamma(1-c)\chi \right) \right] = f_1(\Delta), \quad (23)$$

$$\left[\alpha \left(\frac{c}{(1-\chi)^2} + (1-c) \right) \right]^{-1} \left[\frac{2u}{c} + \alpha \left(c \frac{\chi}{1-\chi} + \Gamma(1-c)\chi \right) \right]^2 = f_2(\Delta), \quad (24)$$

$$- \left[\frac{2u}{c} + \alpha \left(c \frac{\chi}{1-\chi} + \Gamma(1-c)\chi \right) \right] \chi = f_0(\Delta). \quad (25)$$

Here $f_n(\Delta) = \int_{-\infty}^{\Delta} Dz (\Delta - z)^n$ ($n = 0, 1, 2$) with $Dz = \frac{dz}{\sqrt{2\pi}} e^{-z^2/2}$ a standard Gaussian measure. We note that $\phi = \int_{-\infty}^{\Delta} Dz = f_0(\Delta)$ represents the probability of a given species i to survive in the long-term limit, i.e. to attain a fixed point value $x_i = \lim_{t \rightarrow \infty} x_i(t) > 0$. We will refer to ϕ as the fraction of surviving species in the following. For $c = 1$ Eqs. (23, 24, 25) are identical to those found in replica-symmetric studies of the statics of the fully connected model [12, 13]. For $\Gamma = 1$ they also coincide with the replica results reported in [13] for the model with symmetric dilution (up to a suitable re-scaling of α in terms of c). Eqs. (23, 24, 25) are readily solved numerically (in terms of λ , q and χ) for all values of the model parameters.

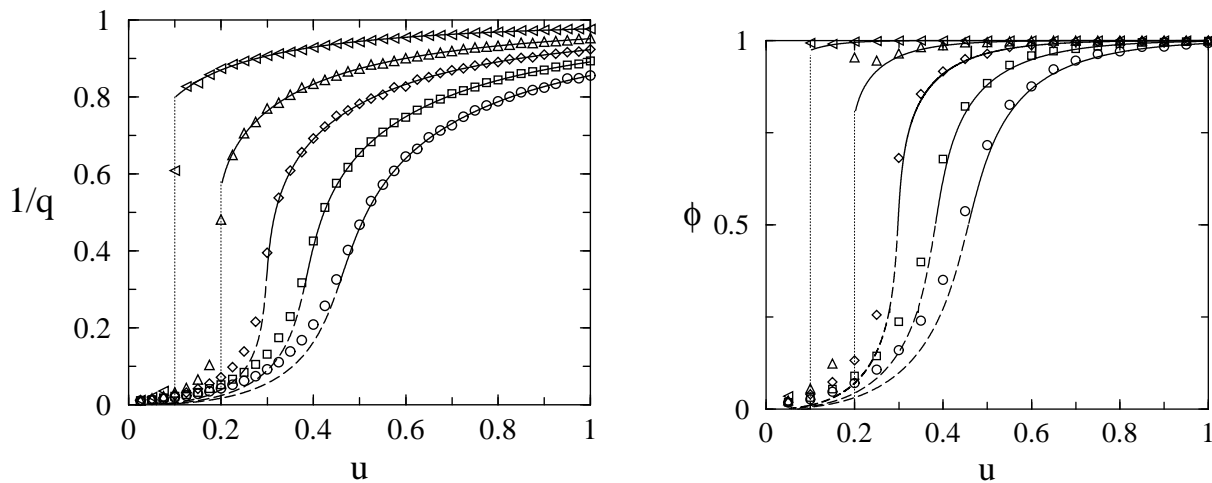


Figure 1. Reciprocal of the persistent correlation q and fraction of surviving species ϕ vs u for different values of α . Solid lines are the analytical predictions for the ergodic phase $u > u^*(\alpha, c, \Gamma)$. For $\alpha > 1/2$ they have been continued into the phase with long-term memory and finite χ as dashed lines (where the ergodic theory is no longer valid). Vertical dotted lines mark the discontinuous transitions at $u = \alpha/2$ for $\alpha < 1/2$. Symbols are from simulations (circles: $\alpha = 1$, squares: $\alpha = 0.8$, diamonds: $\alpha = 0.6$, triangle up: $\alpha = 0.4$, left triangle: $\alpha = 0.2$). Simulations are performed for $N = 300$ species, data are averages over 50 samples of the disorder (20 samples for the fraction of surviving species). The discretisation method used here is that of [8], with effective time-step $\Delta t = [c + N^{-1} \sum_i x_i(t) f_i(t)]^{-1}$ at time t . We here use $c = 10$, the discretised dynamics is iterated for 20000 steps. Dynamics is started from independent random initial conditions drawn from a flat distribution over the interval $x_i(0) \in [0, 2]$.

The resulting predictions for the order parameters q and ϕ for the fully connected case $c = 1$ are tested against numerical simulations of the process (1) in Fig. 1 (the dilute case will be discussed below) ¶, and we observe near perfect agreement in the regime of large values of u , greater than a critical value $u = u^*$. The numerical value of u^* will in general depend on the model parameters α, c and Γ . $u^* = u^*(\alpha, c, \Gamma)$ will be determined analytically in the following section. Below $u^*(\alpha, c, \Gamma)$ systematic deviations from the ergodic theory are observed, the reason for these will become clear below. We attribute small discrepancies between theory and simulations at values $u \geq u^*$ close to the transition points u^* to finite-size or finite-running time effects or to numerical errors due to the discretisation of the original continuous-time replicator dynamics. We would like to point out that Eqs. (23)-(25) admit another (unphysical) solution in the fully connected case for $\alpha < 1/2$ and intermediate values of u , which are not shown in the

¶ Note that extinct species die out only asymptotically, $\lim_{t \rightarrow \infty} x_i(t) = 0$, so that $x_i(t)$ remains positive for all i at finite simulation times t . The fraction of surviving species plotted in Fig. 1 is measured by applying a condition $x_i > \vartheta$ at the end of the simulation runs. We have tested several values of ϑ and slight variations of ϕ appear hard to avoid as ϑ is varied. For the data in Fig. 1 a value of $\vartheta = 0.01$ was used.

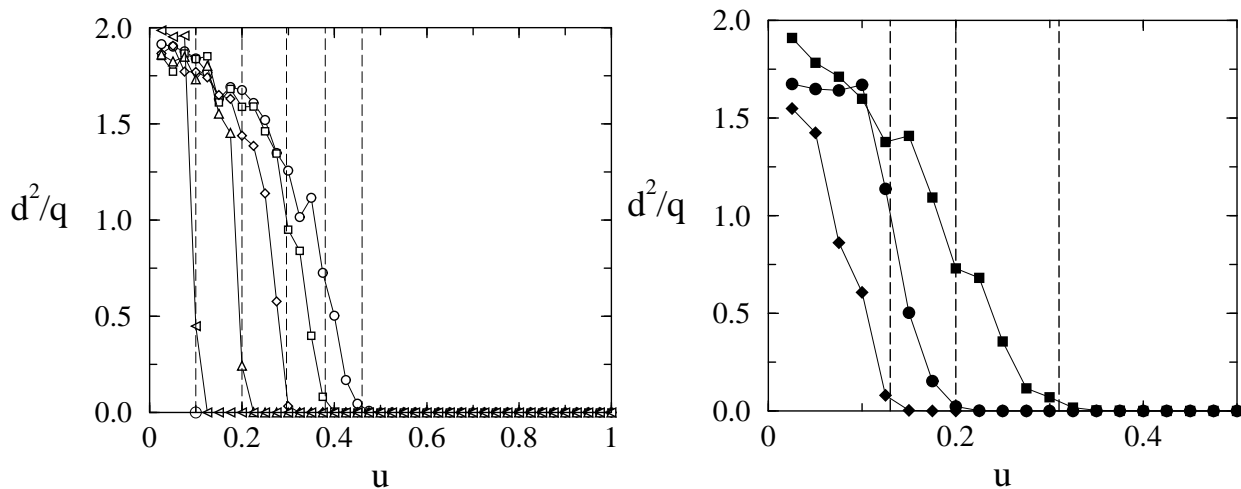


Figure 2. Reduced distance d^2/q between stationary states obtained for a fixed realization of the disorder, but started from independent initial conditions. The connected markers represent results from simulations. Left panel: fully connected model (circles: $\alpha = 1$, squares: $\alpha = 0.8$, diamonds: $\alpha = 0.6$, triangle up: $\alpha = 0.4$, left triangle: $\alpha = 0.2$), right panel: model with dilution (with $(\alpha, c, \Gamma) = (1, 0.5, 0), (1, 0.5, 1), (1, 0.25, 0.5)$ for filled circles, squares and diamonds respectively. Simulation parameters as in Fig. 1, $N = 400$ species for the dilute systems. The vertical dashed lines in both panels indicate the locations of the ergodic/non-ergodic phase transitions as predicted by the analytical theory.

figure.

4. Memory onset and phase diagram

The ansatz we made to address the stationary states implies an explicit assumption regarding the ergodicity of the system. In particular our theory applies only in a regime in which the system does not exhibit any long term memory and in which stationary state does not depend on initial conditions. Apart from being locally stable we therefore require the fixed point reached in the stationary state to be unique. To test this assumption we have performed simulations in which one realization of the disorder is fixed and the system is then started from two different random initial conditions $\{x_i(0)\}$ and $\{x'_i(0)\}$ (with all $x_i(0), x'_i(0)$ drawn from a flat distribution over the interval $[0, 2]$). We depict the resulting distance $d^2 = N^{-1} \sum_i (x_i - x'_i)^2$ between the two fixed points $\{x_i\}$ and $\{x'_i\}$ reached in the long-term limit in Fig. 2 (we normalize by q for convenience). In an ergodic state without memory we expect this distance to vanish, so that initial conditions are irrelevant for the stationary state. As shown in Fig. 2 this is indeed the case for large u greater than $u^*(\alpha, c, \Gamma)$, but initial conditions become relevant below u^* . This suggests a phase transition between an ergodic phase at large u and a non-ergodic regime at low values of u . We will now proceed to compute the critical value $u^*(\alpha, c, \Gamma)$ separating these two regimes analytically.

4.1. Diverging integrated response

A breakdown of our ergodic theory may be signalled by a violation of either of the assumptions we made to address the stationary states. We will first inspect the requirement that the integrated response χ be finite. Taking the limit $\chi \rightarrow -\infty$ (recall $\chi < 0$) in Eq. (25) shows that such a divergence can occur at finite u only for $\Gamma = 0$ or in the fully connected case $c = 1$ and directly leads to $u = \alpha c^2/2$. On the other hand the combination of Eqs. (24) and (25) in the limit $\chi \rightarrow -\infty$ implies

$$\frac{1}{\alpha c} = \frac{f_2(\Delta)}{(f_0(\Delta))^2}. \quad (26)$$

Noting that the ratio on the right-hand-side takes only values greater or equal than 2 (the minimum is attained for $\Delta = 0$), we conclude that a divergence of χ may occur only for $\alpha c \leq 1/2$.

For $c = 1$ such a singularity is indeed observed in the numerical solutions of Eqs. (23,24,25), precisely at the point where discontinuities in the order parameters occur at $u^* = \alpha/2$ in our simulations for $\alpha < 1/2$, see Fig. 1. For $\alpha > 1/2$ no divergence of the integrated response is found. In the model with dilution ($c < 1$) no such singularity is observed, for $\Gamma > 0$ it is excluded by the arguments given above, for $\Gamma = 0$ it is preceded by a different type of transition, as we will discuss below.

It is in general very tedious to measure response functions directly in simulations. To confirm the predicted divergence of χ in the fully connected model $c = 1$, we therefore note that in the course of the generating functional calculation the covariance matrix $\Lambda(t, t') = \langle \eta(t)\eta(t') \rangle_* / \alpha = [(\mathbb{I} - \mathbf{G})^{-1} \mathbf{C} (\mathbb{I} - \mathbf{G}^T)^{-1}]_{tt'}$ of the effective-species noise also turns out to indicate the temporal correlations of the following order parameters⁺:

$$m^\mu(t) \equiv \frac{1}{\sqrt{N}} \sum_{i=1}^N \xi_i^\mu x_i(t). \quad (27)$$

More precisely one has

$$\Lambda(t, t') = \frac{1}{\alpha N} \sum_{\mu=1}^{\alpha N} \langle m^\mu(t) m^\mu(t') \rangle_*. \quad (28)$$

At the fixed point in the ergodic regime we therefore have (with $m^\mu = \lim_{t \rightarrow \infty} m^\mu(t)$)

$$M \equiv \frac{1}{\alpha N} \sum_{\mu=1}^{\alpha N} \langle (m^\mu)^2 \rangle_* = \frac{q}{(1 - \chi)^2}. \quad (29)$$

In particular we expect $M \rightarrow 0$ as $\chi \rightarrow -\infty$ at $u = \alpha/2$ for $\alpha < 1/2$. This is indeed confirmed in simulations, see Fig. 3. No zeroes of M are observed for any value of u when $\alpha > 1/2$.

⁺ Note that the parameter $m^\mu(t) = N^{-1/2} \sum_i \xi_i^\mu x_i(t)$ is closely related to what is known as an ‘overlap parameter’ in the context of neural networks.

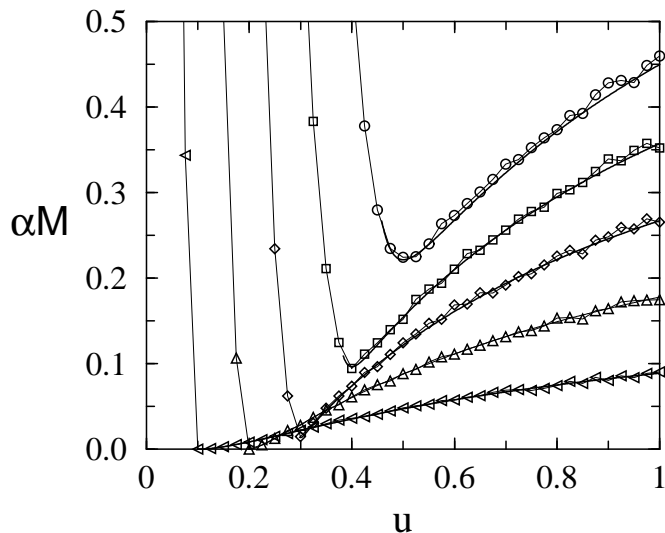


Figure 3. Overlap parameter αM vs u in the fully connected model ($c = 1$) for different values of α . Solid lines are the analytical predictions (29) for the ergodic phase $u > u^*(\alpha, c, \Gamma)$. Connected markers represent results from simulations (circles: $\alpha = 1$, squares: $\alpha = 0.8$, diamonds: $\alpha = 0.6$, triangle up: $\alpha = 0.4$, left triangle: $\alpha = 0.2$). Simulation parameters as in Fig. 1.

4.2. Instability of the fixed point

In this section we will discuss the local stability of the fixed point reached by the system. To this end we will follow [7] and take into account small fluctuations $y(t)$ about the fixed point x attained by the effective species, i.e. we will write $x(t) = x + \varepsilon y(t)$ in Eq. (11), and will accordingly also assume that the single-particle noise is of the form $\eta(t) = \eta + \varepsilon v(t)$, with $v(t)$ a (time-dependent) fluctuation about the fixed point value η . The magnitude of these fluctuations ε is taken to be small. We will also allow for additional white noise $\varepsilon \zeta(t)$ of a small amplitude ε (with $\langle \zeta(t) \zeta(t') \rangle = \delta(t - t')$), and will then study the stability of the fixed point (x, η) with respect to these fluctuations. Note that self-consistency (cf. Eq. (12)) dictates that

$$\langle v(t)v(t') \rangle = \alpha [c(\mathbb{I} - \mathbf{G})^{-1} \mathbf{D}(\mathbb{I} - \mathbf{G}^T)^{-1} + (1 - c)\mathbf{D}](t, t'), \quad (30)$$

where we write $D(t, t') = \langle y(t)y(t') \rangle_*$.

We first note that these fluctuations decay exponentially for species which are dying out asymptotically, i.e. for whom the fixed point is given by $x = 0$. In this case insertion of $x(t) = \varepsilon y(t)$ and $\eta(t) = \Sigma z + \varepsilon v(t)$ into (11) gives (to linear order in ε)

$$\frac{d}{dt} y(t) = -y(t) (\Sigma z - \lambda), \quad (31)$$

and we have $\Sigma z - \lambda > 0$ for fixed points $x(z) = 0$ as seen in (21).

For fixed points $x = x(z) > 0$ we find instead (again to linear order in ε)

$$\frac{d}{dt} y(t) = -x \left(\frac{2u}{c} y(t) + \alpha \int_0^t dt' [c\mathbf{G}(\mathbb{I} - \mathbf{G})^{-1} + \Gamma(1 - c)\mathbf{G}](t, t') y(t') + v(t) + \zeta(t) \right), \quad (32)$$

which is conveniently expressed in terms of Fourier transforms $\{\tilde{y}(\omega), \tilde{v}(\omega), \tilde{\zeta}(\omega), \tilde{G}(\omega)\}$ of $\{y(t), v(t), \zeta(t), G(t)\}$ as

$$\tilde{y}(\omega) = -\frac{\tilde{v}(\omega) + \tilde{\zeta}(\omega)}{i\omega/x + 2u/c + \alpha c \tilde{G}(\omega)/(1 - \tilde{G}(\omega)) + \alpha(1 - c)\Gamma \tilde{G}(\omega)}. \quad (33)$$

Focusing on $\omega = 0$ and using $\langle \zeta(t)\zeta(t') \rangle_\star = \delta(t - t')$ as well as

$$\langle |\tilde{v}(0)|^2 \rangle_\star = \alpha \langle |\tilde{y}(0)|^2 \rangle_\star \left(\frac{c}{(1 - \chi)^2} + (1 - c) \right) \quad (34)$$

(which follows from (30)) we have

$$\tilde{D}(0) \equiv \langle |\tilde{y}(\omega = 0)|^2 \rangle_\star = \frac{\phi \left(\alpha \tilde{D}(0) [c(1 - \chi)^{-2} + (1 - c)] + 1 \right)}{[2u/c + \alpha c \chi / (1 - \chi) + \alpha(1 - c)\Gamma \chi]^2}, \quad (35)$$

where $\tilde{D}(\omega)$ is the Fourier transform of the correlation function $D(\tau) = \langle y(t + \tau)y(t) \rangle_\star$ in the stationary state. The factor ϕ (the fraction of surviving species) takes into account the earlier result that perturbations $y(t)$ about fixed points $x = 0$ do not contribute to the long-time behaviour of the correlation function D . We then find

$$\tilde{D}(0) = \left[\phi^{-1} \left(2u/c + \alpha c \frac{\chi}{1 - \chi} + \alpha \Gamma (1 - c) \chi \right)^2 - \alpha (c(1 - \chi)^{-2} + (1 - c)) \right]^{-1}, \quad (36)$$

so that $\tilde{D}(\omega = 0) = \langle |\tilde{y}(\omega = 0)|^2 \rangle_\star$ diverges when the square bracket on the right-hand-side becomes zero. This condition defines a transition point $u = u^*(\alpha, c, \Gamma)$ and the divergence of $\tilde{D}(\omega = 0)$ at u^* suggests that the assumed fixed points become unstable. $\tilde{D}(\omega = 0)$ is predicted to become negative below the transition, when $\left(2u/c + \alpha c \frac{\chi}{1 - \chi} + \Gamma(1 - c)\chi \right) < \phi \alpha (c(1 - \chi)^{-2} + (1 - c))$, leading to a further contradiction and indicating that our theory cannot be continued below u^* . Using saddle point equation (25) this onset of instability occurs when

$$\frac{\alpha}{\phi} \left(c \frac{\chi^2}{(1 - \chi)^2} + (1 - c)\chi^2 \right) = 1. \quad (37)$$

For $c = 1$ this relation is identical to the condition marking the onset of a de Almeida-Thouless (AT) instability of the replica symmetric solution identified in the analysis of the statics of the fully connected model [13].

4.3. Breakdown of weak-long term memory

While in the previous section we have related the breakdown of our ergodic theory to a local instability of the fixed point reached by the dynamics, we will now inspect for an onset of long-term memory at finite integrated response. This type of transition has

* Further details regarding this type of transition can also be found in [7, 8]: Instabilities of the above type have been associated with $1/\omega$ (or similar) divergencies of $D(\omega)$ at the transition point $u = u^*(\alpha, c, \Gamma)$ as $\omega \rightarrow 0$ in Gaussian replicator models, indicating that fluctuations $y(t)$ are no longer damped and the fixed points become unstable at $u = u^*(\alpha, c, \Gamma)$. Above the transition $\langle y(t + \tau)y(t) \rangle_\star$ decays as $1/\tau^2$ as $\tau \rightarrow \infty$, suggesting that the fixed points are local attractors of the dynamics.

been observed previously for example in Minority Games with self-impact correction or diluted interactions [24, 25], and can also be interpreted in terms of a breakdown of time-translation invariance, see [2] for details. In order to see how solutions with memory bifurcate from the time-translation invariant ergodic states we will make the following ansatz for the response function

$$G(t, t') = G_0(t - t') + \varepsilon \widehat{G}(t, t'), \quad (38)$$

where $\varepsilon \widehat{G}(t, t')$ is a small contribution which breaks time-translation invariance. In the context of the present replicator model the time-translation invariant part \mathbf{G}_0 reflects the contribution of the surviving species to the total response function as discussed above. Note that asymptotically extinct species do not contribute to the response in time-translation invariant states, as fixed points $x_i = 0$ are insensitive to small perturbations as seen in the previous section. Perturbations applied during the transients of the dynamics, however, can leave their traces in the choice of the particular overall asymptotic fixed point $\mathbf{x} = (x_1, \dots, x_N)$: the specific set of surviving species and their stationary concentrations may well depend on those early perturbations. This effect is accounted for by the function $\widehat{G}(t, t') = \widehat{G}(t')$, which is taken to depend only on the time t' at which the perturbation is applied, but not on the later time t at which the effect of the perturbation is measured [2].

Starting from (38) one expands the kernel of the retarded self-interaction in the effective process to linear order in \widehat{G} , and finds

$$c\mathbf{G}(1 - \mathbf{G})^{-1} + \Gamma(1 - c)\mathbf{G} = c\mathbf{G}_0(1 - \mathbf{G}_0)^{-1} + \Gamma(1 - c)\mathbf{G}_0 + \varepsilon\mathbf{R} + \mathcal{O}(\varepsilon^2), \quad (39)$$

where

$$R(t, t') = \Gamma(1 - c)\widehat{G}(t, t') + c \sum_{n=0}^{\infty} \sum_{m=0}^{n-1} \left[(\mathbf{G}_0)^m \widehat{\mathbf{G}}(\mathbf{G}_0)^{n-m-1} \right] (t, t'). \quad (40)$$

Taking into account this extra contribution we find that fixed points are now to be determined as (with $\chi = \sum_t G_0(t)$)

$$x = \frac{\lambda - \eta - \varepsilon\alpha \int_0^t dt' R(t, t')x(t')}{2u/c + \alpha c\chi/(1 - \chi) + \alpha\Gamma(1 - c)\chi} \theta \left[\lambda - \eta - \varepsilon\alpha \int_0^t dt' R(t, t')x(t') \right]. \quad (41)$$

Taking the derivative with respect to a perturbation at time t'' followed by averaging we then have (to first order in ε)

$$\widehat{G}(t'') = -\frac{\alpha}{2u/c + \alpha c\chi/(1 - \chi) + \alpha\Gamma(1 - c)\chi} \int_0^t dt' R(t, t') \left\langle \theta[\lambda - \eta] \frac{\delta x(t')}{\delta h(t'')} \right\rangle_{\star}. \quad (42)$$

Within our ansatz the average on the right-hand-side is identified as $G_0(t', t'')$. Using the above expression for \mathbf{R} and introducing the shorthand $\widehat{\chi} = \sum_t \widehat{G}(t)$ we then find (after suitable integration over t'' and averaging over t)

$$\widehat{\chi} = -\frac{\alpha}{2u/c + \alpha c\chi/(1 - \chi) + \alpha\Gamma(1 - c)\chi} \left(c \frac{\chi}{(1 - \chi)^2} + \Gamma(1 - c)\chi \right) \widehat{\chi}. \quad (43)$$

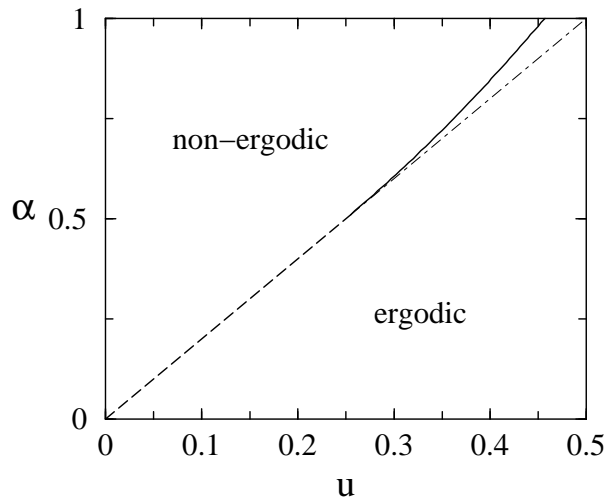


Figure 4. Phase diagram of the model. The dashed line $u = \alpha/2$ for $\alpha < 1/2$ marks the discontinuous transition signalled by a divergence of the integrated response. The solid line for $\alpha > 1/2$ corresponds to the simultaneous onset of long-term memory and of an instability of the fixed point against small perturbations. The line $u = \alpha/2$ has been continued as a dot-dashed line for $u > \alpha/2$.

Although $\hat{\chi} = 0$ is always a solution, non-zero branches may bifurcate from the time-translation invariant solution at the point at which the coefficient in front of $\hat{\chi}$ on the right-hand-side of (43) becomes one. Using Eq. (25) this condition is given by

$$\frac{\alpha}{\phi} \left(c \frac{\chi^2}{(1-\chi)^2} + \Gamma(1-c)\chi^2 \right) = 1. \quad (44)$$

For fully symmetric dilution ($\Gamma = 1$) this is identical to the above condition (37) marking the onset of the instability of the fixed points and for $c = 1$ furthermore coincides with the condition signalling the AT-instability of the replica-symmetric solutions of the statics of the fully connected model [12, 13]. For $\Gamma < 1$ (and $c < 1$) one observes that a fulfillment of memory-onset condition (44) implies that the instability of the fixed points has already set in (as signalled by a negative right-hand-side of (36)). For asymmetrically diluted couplings the onset of instability thus occurs first as u is lowered at fixed α, c, Γ and the MO-line (44) has no physical meaning. A physical interpretation of the two types of transitions in the case of (partially) asymmetric dilution will be discussed briefly below.

4.4. Phase diagram of the fully connected model

The resulting phase diagram of the fully connected model ($c = 1$) in the (u, α) -plane is shown in Fig. 4 and coincides with the one found in the statics [12, 13]. For values of α greater than $1/2$ we do not find any divergence of any of the order parameters, but rather a continuous onset of long-term memory occurs at a point $u^* = u^*(\alpha)$ slightly above the line $u = \alpha/2$, accompanied by a simultaneous onset of an instability of the

assumed fixed point against small fluctuations. All order parameters are continuous across this transition.

For $\alpha < 1/2$ one finds a divergence $\chi \rightarrow -\infty$ at $u^*(\alpha) = \alpha/2$ as discussed above. This transition is marked by discontinuities in the order parameters such as q and ϕ , see Fig. 1. We also note that the overlap parameter M vanishes at this point $u = u^*(\alpha)$ for $\alpha < 1/2$, but that simulations suggest that it remains strictly positive below this transition ($u < u^*(\alpha)$) as indicated in Fig. 3. This is at variance with the behaviour of the analogous quantity H in Minority Games [1, 2], which is positive above the corresponding transition of the Minority Game, vanishes at the point at which χ diverges and then remains identically zero below the transition point[‡]. In simulations (not shown here) we also do not observe any discontinuities of q or ϕ as α is varied at constant u strictly within in the non-ergodic phase (i.e. not crossing the line segment $u = \alpha/2$, $0 \leq \alpha \leq 1/2$). In this sense the non-ergodic phase indicated in Fig. 4 does not appear to be divided into two separate regions in an obvious way (for example one with $\chi = -\infty$, $M = 0$ and another with χ finite and $M > 0$).

As shown in Figs. 1 and in the left panel of Fig. 2 the analytically obtained location $u^*(\alpha, c = 1)$ of the phase transition in the fully connected model agrees (within the accuracy of our simulations) with the onset of deviations from the ergodic theory and of the sensitivity to initial conditions ^{††}++.

The general picture that emerges here seems to indicate that in the ergodic regime $u > u^*(\alpha, c = 1)$ only one fixed point is found, so that the microscopic dynamics ends up in the same configuration independently of initial conditions. Below $u^*(\alpha, c = 1)$ all trajectories still evolve into microscopic fixed points, but these do not seem to be unique, but possibly of an exponential (in N) number [6, 7], leading to the identified dynamic instabilities and the breaking of ergodicity (and to a breakdown of the replica-symmetric solution in the statics). Further studies of the non-ergodic regime, possibly along the lines of [6] might however be appropriate to understand the nature of this phase in more detail. Given the memory effects below u^* an analysis of the dynamics below the transition is very likely to require a solution in terms of the full two-time quantities $C(t, t')$ and $G(t, t')$ during the transients of the system's temporal evolution.

[‡] The so-called ‘predictability’ H studied in Minority Games is analogous to the overlap parameter M discussed here in the sense that both quantities are proportional to the covariance of the effective single-particle noises of the respective models at infinite time-separation.

^{††}Note that d^2 as depicted in Fig. 2 is a measure for the distance between the microscopic fixed points reached from different realisations of the random initial conditions. In contrast to Minority Games where the so-called ‘market volatility’ crucially depends on the starting point in the non-ergodic regime of the game we have not been able to identify an observable which can be expressed in terms of the dynamic order parameters $\{\mathbf{C}, \mathbf{G}\}$ (and possibly $\boldsymbol{\lambda}$) and which shows a dependence on the type of initial conditions below u^* .

⁺⁺Note also that in [24] *small* perturbations were applied in a similar situation in the context of the Minority Game to verify the onset of memory. We have tried to measure the response of the present system to small perturbations at early and late times respectively, but found the resulting simulations to be inconclusive. The data in Fig. 2 is therefore restricted to separate starts from two independent sets of initial conditions at fixed disorder.

4.5. Effects of dilution

We will now turn to the consequences of diluting the Hebbian couplings. A brief discussion of these effects can also be found in [13], albeit based on replica methods and hence restricted to the case of symmetric dilution.

First note that the relations (37) and (44) signalling the instability of the fixed points and the onset of memory respectively coincide for symmetric dilution $\Gamma = 1$. In this case a Lyapunov function of the replicator dynamics can be found and the system evolves into a fixed point irrespective of $\{u, \alpha, c\}$. Below $u^*(\alpha, c, \Gamma = 1)$ exponentially many fixed points exist and initial conditions as well as perturbations in the transients determine which of these is reached by the dynamics, resulting in broken ergodicity and memory effects. For $\Gamma < 1$ the instability condition (37) is fulfilled first as u is lowered from large values (at constant $\alpha, c, \Gamma < 1$). While above u^* one single stable fixed point is found, the number of fixed points is expected to be exponentially (in N) suppressed for asymmetric couplings below the transition [7, 8]. Since no phase with multiple fixed points is found for $\Gamma < 1$ no MO-transition occurs (the identification of which was based on a fixed-point assumption also below u^*) and the line in the phase diagram defined by (44) has no physical meaning as it is preceded by condition (37). The relation between the MO- and instability condition is discussed in more detail also in [26]. Furthermore no singularities $\chi \rightarrow -\infty$ are found for $c < 1$ before the instability condition sets in, resulting in the location of all transitions being determined by (37) in this case.

The phase diagrams for fully symmetric and fully asymmetric dilution are shown in Fig. 5. With the present scaling of the self-interactions (with c) the general effect of increasing dilution appears to be an increase the range of ergodicity, only in a region directly below the transition line of the fully connected model do we find re-entrance behaviour: here the system is ergodic at $c > c_2$ and fixed (u, α) , becomes non-ergodic at in an intermediate interval $c \in [c_1, c_2]$ and then ergodic again for $c < c_1$. We have performed some simulations to confirm these findings (not shown here). While the numerical experiments are consistent with re-entrance behaviour the exact location of the window of non-ergodicity is hard to verify numerically especially because c_2 is found to lie close to $c = 1$ in the analytical solution.

Finally we plot the reciprocal order parameter $1/q$ versus the connectivity c at fixed (u, α, Γ) in Fig. 6. While the scaling of the self-interaction used here, both purely decreasing behaviour with increasing connectivity as well as extremal diversity at intermediate c can be found depending on the values of u and α . Similar non-monotonic behaviour is also reported in [13] for the case of symmetric dilution, although we note here that adapting our theory to a model with $J_{ii}c_{ii}/c = \mathcal{O}(c^0)$ suggest that this non-monotonicity and the above re-entrance effects appear are to be absent if the self-interaction does not scale with c (results not shown). In general one observes that the diversity $1/q$ (and the fraction of surviving species) is higher for asymmetric than for symmetric dilution.

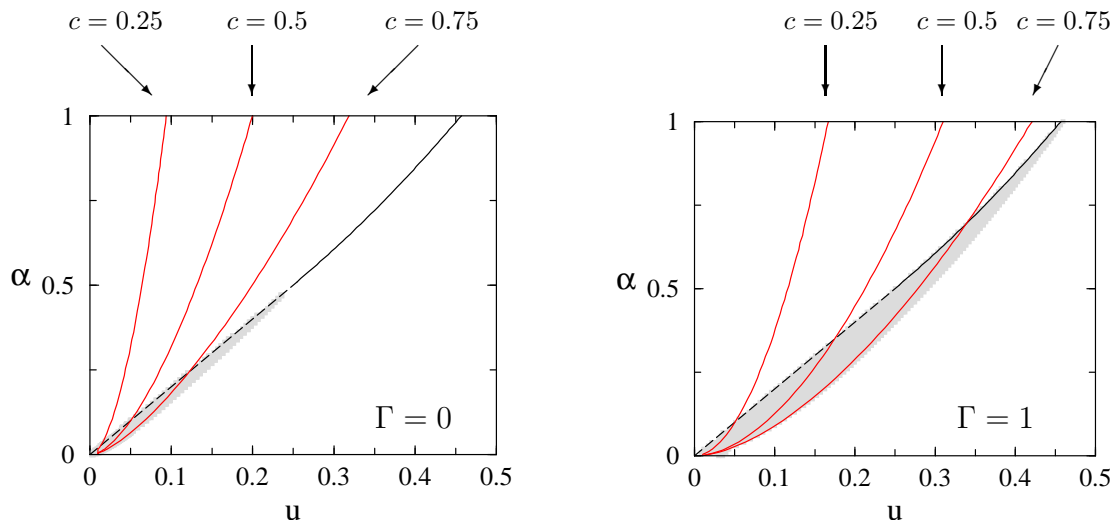


Figure 5. Phase diagrams of the models with fully asymmetric and with fully symmetric dilution. The curves in the (u, α) -plane mark the onset of memory at constant $c = 0.25, 0.5, 0.75$. Ergodic phases are found to the bottom-right of the curves. The transition line of the fully connected model $c = 1$ is shown for comparison. The grey areas are sketches of the re-entrance regions, here the system is ergodic for small $c \ll 1$, non-ergodic in an intermediate regime and ergodic again at large c close to $c = 1$.

5. Finite number of traits

We now turn to the case of a finite number p of traits. In this case generating functionals are not required to formulate a closed dynamical theory, instead it is sufficient to study the evolution of the probability distributions of species concentrations on so-called sublattices, in which all species with the same trait vector $\xi_i = (\xi_i^{\mu=1}, \dots, \xi_i^{\mu=p})$ are treated collectively. We here concentrate on the fully connected model.

The replicator equations take the form

$$\frac{d}{dt}x_i(t) = -x_i(t) \left(\sum_j J_{ij}x_j(t) - \frac{1}{N} \sum_{jk} J_{jk}x_j(t)x_k(t) \right) \quad (45)$$

with

$$J_{ij} = N^{-1} \sum_{\mu=1}^p \xi_i^\mu \xi_j^\mu, \quad i \neq j, \quad J_{ii} = 2u. \quad (46)$$

It is known from the statics that a model with a finite number of traits chosen with equal probability from $\xi_i^\mu \in \{-1, 1\}$ leads to a trivial stationary state (with fixed points $x_i \equiv 1$ for all i) [11] so that we follow [11] and introduce a bias parameter $a \in [0, 1]$ and draw the traits independently from a distribution

$$P(\xi_i^\mu) = \frac{1+a}{2} \delta_{\xi_i^\mu, 1} + \frac{1-a}{2} \delta_{\xi_i^\mu, -1} \quad (47)$$

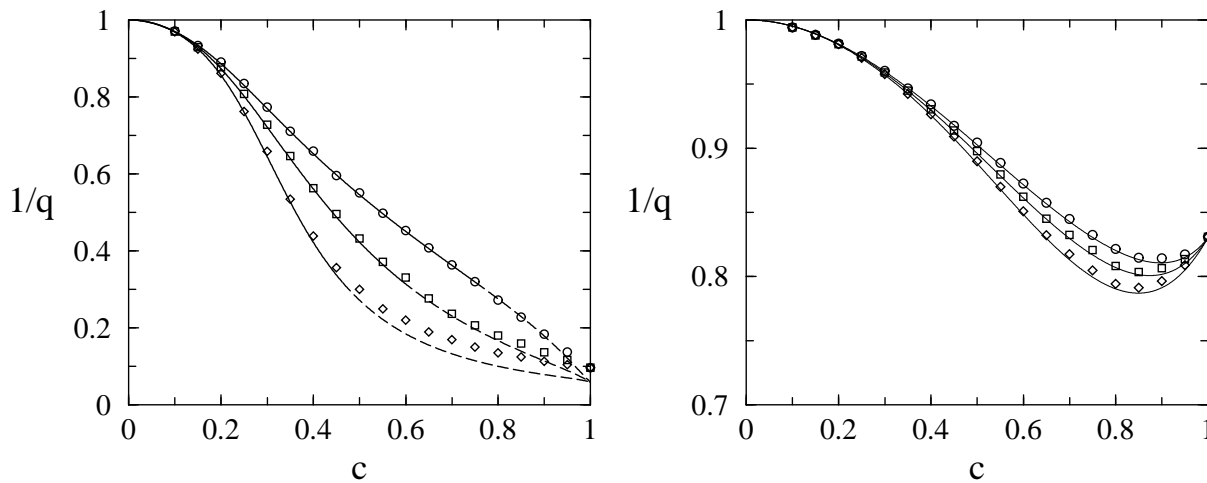


Figure 6. Inverse order parameter $1/q$ at fixed (u, α, Γ) as a function of the connectivity for the dilute system. Left: $u = 0.2, \alpha = 0.5$, right: $u = 0.5, \alpha = 0.5$. Solid lines are obtained from the ergodic theory and have been continued as dashed lines into the non-ergodic phase. Symbols are from simulations with $N = 500$ species, run for 20000 discretisation steps, averaged over 50 samples of the disorder (circles: $\Gamma = 0$, squares: $\Gamma = 0.5$, diamonds: $\Gamma = 1$).

for all i and μ .

Analytical progress can here be made without the use of generating functionals. It is sufficient to introduce sub-lattices

$$I_{\boldsymbol{\eta}} = \{i : \boldsymbol{\xi}_i = \boldsymbol{\eta}\} \subset \{1, \dots, N\} \quad (48)$$

with $\boldsymbol{\eta} \in \{-1, 1\}^p$ and to consider the macroscopic observables

$$\rho_{\boldsymbol{\eta}}(x, t) = \left\langle |I_{\boldsymbol{\eta}}|^{-1} \sum_{i \in I_{\boldsymbol{\eta}}} \delta(x - x_i(t)) \right\rangle, \quad (49)$$

in terms of which closed dynamical equations can be formulated along the lines of [19]. $\langle \dots \rangle$ here denotes an average with respect to the time-dependent microscopic state density $p_t(x_1, \dots, x_N)$. With the relative proportions $p_{\boldsymbol{\eta}} = \lim_{N \rightarrow \infty} |I_{\boldsymbol{\eta}}|/N$ the Fokker-Planck equation governing the evolution of $p_t(x_1, \dots, x_N)$ can be reduced to the following set of 2^p equations closed in the 2^p probability distributions $\{\rho_{\boldsymbol{\eta}}(x, t) : \boldsymbol{\eta} \in \{-1, 1\}^p\}$, valid in the thermodynamic limit $N \rightarrow \infty$:

$$\frac{d}{dt} \rho_{\boldsymbol{\eta}}(x) = - \frac{\partial}{\partial x} \left[x \left(-2ux - \sum_{\boldsymbol{\eta}'} p_{\boldsymbol{\eta}'} \boldsymbol{\eta} \cdot \boldsymbol{\eta}' \int dx' \rho_{\boldsymbol{\eta}'}(x') x' \right) \right] \quad (50)$$

$$+ \sum_{\boldsymbol{\eta}', \boldsymbol{\eta}''} p_{\boldsymbol{\eta}'} p_{\boldsymbol{\eta}''} \boldsymbol{\eta}' \cdot \boldsymbol{\eta}'' \int dx' \rho_{\boldsymbol{\eta}'}(x') x' \int dx'' \rho_{\boldsymbol{\eta}''}(x'') x'' \quad (51)$$

$$\left. + 2u \sum_{\boldsymbol{\eta}'} p_{\boldsymbol{\eta}'} \int dx' \rho_{\boldsymbol{\eta}'}(x') x'^2 \right]. \quad (52)$$

We have here suppressed the time-dependence of the densities $\rho_{\boldsymbol{\eta}}(x)$ and use the shorthand $\boldsymbol{\eta} \cdot \boldsymbol{\eta}' = \sum_{\mu=1}^p \eta_{\mu} \eta'_{\mu}$. Upon the introduction of the moments

$$\nu_{\boldsymbol{\eta}}^{(k)}(t) = \int_0^{\infty} dx \rho_{\boldsymbol{\eta}}(x) x^k \quad (53)$$

($k = 0, 1, 2, \dots$) one has

$$\begin{aligned} \frac{d}{dt} \rho_{\boldsymbol{\eta}}(x) = & - \frac{\partial}{\partial x} \left[x \left(-2ux - \sum_{\boldsymbol{\eta}'} p_{\boldsymbol{\eta}'} \boldsymbol{\eta} \cdot \boldsymbol{\eta}' \nu_{\boldsymbol{\eta}'}^{(1)} \right. \right. \\ & \left. \left. + \sum_{\boldsymbol{\eta}', \boldsymbol{\eta}''} p_{\boldsymbol{\eta}'} p_{\boldsymbol{\eta}''} \boldsymbol{\eta}' \cdot \boldsymbol{\eta}'' \nu_{\boldsymbol{\eta}'}^{(1)} \nu_{\boldsymbol{\eta}''}^{(1)} + 2u \sum_{\boldsymbol{\eta}'} p_{\boldsymbol{\eta}'} \nu_{\boldsymbol{\eta}'}^{(2)} \right) \right]. \end{aligned} \quad (54)$$

Due to the effective non-linearity (in x) on the right-hand-side a simple solution in terms for example of an Ornstein-Uhlenbeck process [19] appears impossible. Multiplication of (54) by x^k on both sides and subsequent integration over x then leads to

$$\frac{d}{dt} \nu_{\boldsymbol{\eta}}^{(k)} = -2k u \nu_{\boldsymbol{\eta}}^{(k+1)} - k \nu_{\boldsymbol{\eta}}^{(k)} \left[\sum_{\mu} \eta_{\mu} m_{\mu} - \sum_{\mu} m_{\mu} m_{\mu} - 2u \sum_{\boldsymbol{\eta}'} p_{\boldsymbol{\eta}'} \nu_{\boldsymbol{\eta}'}^{(2)} \right], \quad (55)$$

with $m_{\mu} = \sum_{\boldsymbol{\eta}} p_{\boldsymbol{\eta}} \eta_{\mu} \nu_{\boldsymbol{\eta}}^{(1)}$. Eqs. (55) form a closed, but hierarchical system of equations for the time-evolution of the moments $\{\nu_{\boldsymbol{\eta}}^{(k)}(t)\}$.

We will now assume symmetrical initial conditions $m_{\mu}(t=0) \equiv m(0)$ for all μ , and will accordingly write $m_{\mu}(t) \equiv m(t)$ for all μ for all times t . Furthermore the densities $\rho_{\boldsymbol{\eta}}(x)$ will depend on the sub-lattice structure only via the number of entries $+1$ in the vector $\boldsymbol{\eta}$, i.e. all indices $\boldsymbol{\eta}$ may effectively be replaced by $n(\boldsymbol{\eta}) = |\{\mu : \eta_{\mu} = 1\}|$, and the $p_{\boldsymbol{\eta}}$ translate into probabilities

$$W_n = \binom{n}{p} \left(\frac{1+a}{2} \right)^n \left(\frac{1-a}{2} \right)^{p-n}, \quad n = 0, 1, 2, \dots, p \quad (56)$$

for the occurrence of a trait vector $\boldsymbol{\eta}$ with n entries equal to $+1$ (and $p-n$ entries equal to -1). The overlap can then be written as

$$m(t) = \sum_{n=0}^p W_n \nu_n^{(1)}(t) \left(\frac{2n}{p} - 1 \right) \quad (57)$$

(where we have used $\lim_{N \rightarrow \infty} |I_{\boldsymbol{\eta}}|^{-1} \sum_{i \in I_{\boldsymbol{\eta}}} \eta_{\mu} = (2n(\boldsymbol{\eta})/p) - 1 \forall \mu$). The dynamical equations for the first two moments simplify to

$$\frac{d}{dt} \nu_n^{(1)} = -2u \nu_n^{(2)} - \nu_n^{(1)} \left[mp \left(\frac{2n}{p} - 1 \right) - pm^2 - 2u \sum_{n'=0}^p W_{n'} \nu_{n'}^{(2)} \right] \quad (58)$$

$$\frac{d}{dt} \nu_n^{(2)} = -4u \nu_n^{(3)} - 2\nu_n^{(2)} \left[mp \left(\frac{2n}{p} - 1 \right) - pm^2 - 2u \sum_{n'=0}^p W_{n'} \nu_{n'}^{(2)} \right]. \quad (59)$$

Note that this set of equations does not close as the evolution of the second moments couples to the third moments, the evaluation of which requires the fourth moments and so on. In general one has

$$\frac{d}{dt}\nu_n^{(k)} = -2k u \nu_n^{(k+1)} - k \nu_n^{(k)} \left[mp \left(\frac{2n}{p} - 1 \right) - pm^2 - 2u \sum_{n'=0}^p W_{n'} \nu_{n'}^{(2)} \right]. \quad (60)$$

A brief remark on the stationary state are in order at this point. Indeed it is straightforward to verify that the static solution $\rho_n(x) = \delta(x - x_n)$ with

$$x_n = 1 + \frac{pa(a+1) - 2an}{2u+1-a^2}, \quad n = 0, 1, \dots, p \quad (61)$$

found in [11] and resulting in $m = 2ua/(2u+1-a^2)$ is a fixed point of the above dynamical equations. We here assume that

$$p < 1 + \frac{1}{a} + \frac{2u}{a(1-a)} \quad (62)$$

so that all species survive in the long-term limit. A more detailed discussion regarding the fraction of surviving species whenever this condition is not fulfilled can be found in [11].

In order to proceed with the analysis of the dynamics an approximation is required at this stage, effectively truncating the above hierarchical set of equations. We here restrict the further discussion to the most simple approximative scheme and take the densities $\rho_n(x)$ to be Gaussian. This allows to express each third moment $\nu_n^{(3)}$ in terms of $\nu_n^{(1)}$ and $\nu_n^{(2)}$ and we find the following approximate but closed set of $2(p+1)$ equations for the $\{\nu_n^{(1)}, \nu_n^{(2)}\}$, $n = 0, 1, \dots, p$:

$$\frac{d}{dt}\nu_n^{(1)} = -2u\nu_n^{(2)} - \nu_n^{(1)} \left[mp \left(\frac{2n}{p} - 1 \right) - pm^2 - 2u \sum_{n'} W_{n'} \nu_{n'}^{(2)} \right] \quad (63)$$

$$\frac{d}{dt}\nu_n^{(2)} = -4u[\nu_n^{(1)}(3\nu_n^{(2)} - 2(\nu_n^{(1)})^2)] - 2\nu_n^{(2)} \left[mp \left(\frac{2n}{p} - 1 \right) - pm^2 - 2u \sum_{n'} W_{n'} \nu_{n'}^{(2)} \right] \quad (64)$$

We will write $\sigma_n^2 \equiv \nu_n^{(2)} - (\nu_n^{(1)})^2$ in the following. The Gaussian approximation can be expected to be accurate at most in a regime where the $\rho_n(x)$ are highly peaked around positive means, i.e. in which $\nu_n^{(1)} > 0$ and $\sigma_n^2/(\nu_n^{(1)})^2 \ll 1$. In particular any Gaussian approximation with $\sigma_n^2 > 0$ is inconsistent in the sense that it assigns finite probability to negative species concentrations, which are excluded *a priori* by the replicator equations. Note however that our approximative ansatz consists only of assuming the relations between the first three moments of Gaussian distributions to hold for the densities $\rho_n(x)$. No other properties of Gaussian distributions are used here.

In regimes in which (62) is fulfilled the numerical solution of (63,64) evolves towards a fixed point $\nu_n^{(1)} = x_n > 0$, $\sigma_n^2 = 0$ asymptotically as shown in Fig. 7 so that the validity of the Gaussian ansatz is verified *a posteriori*. We expect the numerical solution of the approximate equations (63,64) to capture the dynamical behaviour of the system at least in the asymptotic regime of large times. This is indeed confirmed by comparison with

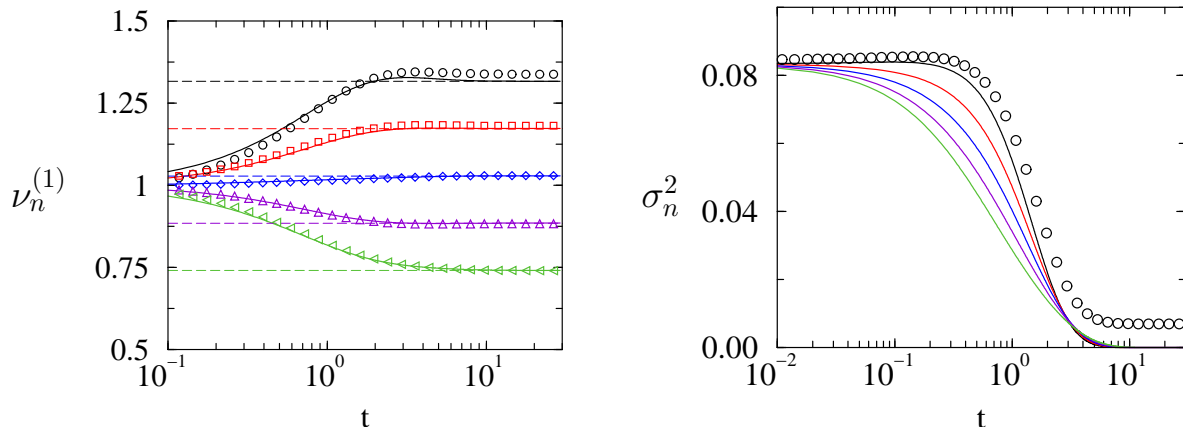


Figure 7. Temporal evolution of the moments $\{\nu_n^{(1)}, \sigma_n^2\}$ (see text for definitions) for the replicator system with $p = 4$ traits at fixed $u = 0.2, a = 0.1$. Solid lines are obtained from a numerical solution of Eqs. (63,64,57) (time-stepping $dt = 10^{-6}$). Different lines are for $n = 0, 1, \dots, 4$ from top to bottom in the left panel and from top to bottom at intermediate times in the right panel. Horizontal lines in the left panel are the fixed point values given by Eq. (61). Symbols are from simulations of the replicator system with $p = 4$ patterns, $N = 300$, averages over 50 samples of the disorder are taken (with circles, squares, diamonds, up and left triangles corresponding to $n = 0, 1, \dots, 4$ respectively; numerical results for the variance (right panel) are shown only for $n = 0$). Initial concentrations are drawn from a flat distribution over the interval $[0.5, 1.5]$, corresponding to $\nu_n^{(1)}(t = 0) = 1$ and $\sigma_n^2(t = 0) = 0.083$ for all $n = 0, \dots, 4$.

measurements of $\nu_n^{(1)}(t)$ in numerical simulations, see the left panel of Fig. 7. (We note here that the width of the distributions $\rho_n(x)$ measured in our numerical experiments appears to remain finite ($\sigma_n^2 \approx 0.01$) up to the time interval covered in simulations as shown in the right panel of Fig. 7. A similar effect was observed in [11], and is presumably due to finite-size or finite running-time effects or to discretisation errors in the numerical scheme used to iterate the replicator equations.)

6. Concluding remarks

To summarise we have used dynamical techniques to study systems of interacting replicators subject to random Hebbian couplings with and without dilution. Our study focuses on the statistical mechanics properties of the model and complements existing replica analyses of the fully connected model. In the fully connected case both approaches lead to the same equations describing the ergodic stationary states of the system and accordingly the phase diagrams obtained from the statics and the dynamics respectively coincide. In addition we have identified two different types of phase transitions and patterns of ergodicity breaking in the fully connected model, one signalled by a diverging integrated response, the other marked by an onset of long-term memory at finite χ as well as by a dynamical instability of the fixed point solutions

against small perturbations. This latter dynamical transition corresponds to an AT-instability of the replica-symmetric solution found in the statics.

The generating functional approach used here allows one to go beyond the models accessible by static replica techniques, and we have extended the analysis to the case of Hebbian couplings with dilution of an arbitrary symmetry. We find that no divergencies of the integrated response occur in diluted models, but that the transition marked by an instability of the fixed points persists. With the scaling of self-interactions used here dilution in general increases the range of ergodic behaviour in the (u, α) -plane, up to a small region of re-entrance. The order parameters show non-trivial behaviour as a function of the connectivity. Asymmetry in the dilutions appears to promote an increased survival probability of any individual species.

Finally we have presented a discussion of the dynamics of a replicator system with a finite number of traits. Techniques developed originally for neural networks can be used to formulate an exact hierarchical set of equations for the concentration-densities on sub-lattices resulting from the quenched assignment of traits. Within a Gaussian ansatz approximate, but closed equations for the evolution of the first two moments of these densities can be found, and allow one to study the approach to the stationary state analytically and in good agreement with numerical simulations.

Several extensions of the present work are possible and of potential interest. While we have here addressed only the case of extensively connected species the phenomenology of the finite-connectivity case $cN \sim \mathcal{O}(1)$ might be worthwhile studying with dynamical methods now becoming available for finite-connectivity systems [27]. Furthermore replicator systems with heterogeneous species-dependent degree of connectivity c_i could be taken into account leading to an ensemble of effective processes [28], as well as the possibility of species not carrying all traits but only a certain individual subset. Finally an ‘on-line’ version of the present model could be devised in discrete time, i.e. one in which at each step only one active trait $\mu(t)$ is relevant for the evolution of the replicator system (as opposed to the present ‘batch’ model in which an effective contraction over all traits is considered).

Acknowledgements

This work was supported by the European Community’s Human Potential Programme under contract HPRN-CT-2002-00319, STIPCO. The author would like to thank D Sherrington for bringing random replicator models to his attention, and A C C Coolen for discussions on dynamical methods. Stimulating interaction with M Bazan Peregrino is gratefully acknowledged.

References

- [1] Challet D, Marsili M and Zhang Y-C 2005 *Minority Games* (Oxford University Press, Oxford UK)
- [2] Coolen A C C 2005 *The Mathematical Theory of Minority Games* (Oxford University Press, Oxford UK)

- [3] Johnson NF, Jefferies P and Hui PM 2003 *Financial market complexity* (Oxford University Press, Oxford UK)
- [4] Hofbauer J, Sigmund K 1988 *Dynamical Systems and the Theory of Evolution* (Cambridge University Press, Cambridge UK)
- [5] Peschel M, Mende W 1986 *The Prey-Predator Model* (Springer Verlag, Vienna)
- [6] Diederich S, Opper M 1989 *Phys. Rev. A* **39** 4333
- [7] Opper M, Diederich S 1992 *Phys. Rev. Lett.* **69** 1616
- [8] Opper M, Diederich S 1999 *Comp. Phys. Comm.* **121-122** 141
- [9] de Oliveira V Fontanari J 2000 *Phys. Rev. Lett.* **85** 4984
- [10] de Oliveira V and Fontanari J 2001 *Phys. Rev. E* **64** 051911
- [11] de Oliveira V and Fontanari J 2002 *Phys. Rev. Lett.* **89** 148101
- [12] de Oliveira V 2003 *Eur. Phys. J. B* **31** 259
- [13] Santos D, Fontanari J 2004 *Phys. Rev. E* **70** 061914
- [14] Tokita K 2004 *Phys. Rev. Lett.* **93** 178102
- [15] Biscari P, Parisi G 1995 *J. Phys. A: Math. Gen.* **28** 4697
- [16] Tokita K, Yasumoti A 1999 *Phys. Rev. E* **60** 842
- [17] Chawanya T, Tokita K 2002 *J. Phys. Soc. Japan* **71** 429
- [18] Coolen A C C 2001, in Handbook of Biological Physics Vol 4 (Elsevier Science, eds F Moss and S Gielen) 513, `cond-mat/0006010`
- [19] Coolen A C C 2001, in Handbook of Biological Physics Vol 4 (Elsevier Science, eds F Moss and S Gielen) 597, `cond-mat/0006011`
- [20] Rieger H 1989 *J. Phys. A: Math. Gen.* **22** 3447
- [21] De Dominicis C, *Phys. Rev. B* **18**, 4913 (1978)
- [22] Crisanti A, Horner H, Sommers H-J 1193 *Z. Phys. B.* **92** 257
- [23] Eissfeller H and Opper M 1992 *Phys. Rev. Lett.* **68** 2094
- [24] Heibel JAF, De Martino A 2001 *J. Phys. A: Math. Gen.* **34** L539
- [25] Galla T 2005 *J. Stat. Mech.* P01002
- [26] Galla T 2005, preprint `cond-mat/0508174`)
- [27] Hatchett J P L, Wemmenhove B, Perez Castillo I, Nikolettopoulos T, Skantzos N S, Coolen A C C 2004 *J. Phys. A: Math. Gen.* **37** 6201
- [28] Galla T, Sherrington D 2005 *Eur. J. Phys. B* **46** 153